Appl Petrochem Res (2013) 3:83–89
DOI 10.1007/s13203-013-0033-y

ORIGINAL ARTICLE

Comparing $Pt/SrTiO_3$ to $Rh/SrTiO_3$ for hydrogen photocatalytic production from ethanol

A. K. Wahab · T. Odedairo · J. Labis · M. Hedhili · A. Delavar · H. Idriss

Received: 22 June 2013 / Accepted: 23 July 2013 / Published online: 13 August 2013

Abstract Photocatalytic hydrogen production from ethanol as an example of biofuel is studied over 0.5 wt% $Rh/SrTiO_3$ and 0.5 wt% $Pt/SrTiO_3$ perovskite materials. The rate of hydrogen production, r_{H2}, over $Pt/SrTiO_3$ is found to be far higher than that observed over $Rh/SrTiO_3$ (4×10^{-6} mol of H_2 $g_{catal.}^{-1}$ min^{-1} (1.1×10^{-6} mol of H_2 $m_{catal.}^{-2}$ min^{-1}) compared to 0.7×10^{-6} mol of H_2 $g_{catal.}^{-1}$ min^{-1} (5.5×10^{-8} mol of H_2 $m_{catal.}^{-2}$ min^{-1}), respectively, under UV excitation with a flux equivalent to that from the sun light (ca. 1 mW cm^{-2}). Analyses of the XPS Rh3d and XPS Pt4f indicate that Rh is mainly present in its ionic form (Rh^{3+}) while Pt is mainly present in its metallic form (Pt^0). A fraction of the non-metallic state of Rh in the catalyst persisted even after argon ion sputtering. The tendency of Rh to be oxidized compared to Pt might be the reason behind the lower activity of the former compared to the later. On the contrary, a larger amount of methane are formed on the Rh containing catalyst compared to that observed on the Pt containing catalyst due to the capacity of Rh to break the carbon–carbon bond of the organic compound.

Keywords Ethanol-photoreaction · XPS Rh3d · XPS Pt4f · Hydrogen production · Perovskite materials · Band gap · $SrTiO_3$ · Carbon–carbon bond dissociation

Introduction

Photo-catalytic production of hydrogen from renewables is poised to be one of its main sources in the future once successful catalytic materials are made possible. The reaction requires the presence of a semiconductor with bang gap energy within the energy of the solar radiation, a conductor such as a noble metal to accept electrons from the conduction band in addition to hydrogen-containing compounds [1]. Ultimately, the desired compound for hydrogen production is water. Next to water are alcohols and, in particular, ethanol because it is provided from biomass and is therefore renewable [2].

$SrTiO_3$ is stable in water as well as in presence of organic compounds; more importantly it endures corrosion under UV excitation and unlike other non oxygen containing compounds is already oxygen terminated and therefore cannot be over oxidized. It has two band gaps: one indirect at 3.25 eV, similar to anatase the perovskite structure with TiO_2, and one direct at 3.75 eV [3]. The indirect band gap is between the upper valence band, mainly composed of O2p, and the empty states Ti3d (t_{2g}). The direct band gap is between O2p and Ti3d (e_g) levels [4] (Fig. 1).

Numerous works have addressed the photo-catalytic activity of $SrTiO_3$ alone, with other transition metals as well as doped with other ions [5–11]. Results differ strongly from one study to the other due to difference in crystallinity, metal dispersion, effect of dopant and reaction conditions. In a recent work [6], the reactivity of $SrTiO_3$ with different particle sizes was tested for hydrogen

Electronic supplementary material The online version of this article (doi:10.1007/s13203-013-0033-y) contains supplementary material, which is available to authorized users.

A. K. Wahab · T. Odedairo · H. Idriss (✉)
SABIC: T&I Riyadh and CRI-KAUST, Riyadh, Saudi Arabia
e-mail: idrissh@sabic.com

J. Labis
KAIN, Riyadh, Saudi Arabia

M. Hedhili · A. Delavar
KAUST, Thuwal, Saudi Arabia

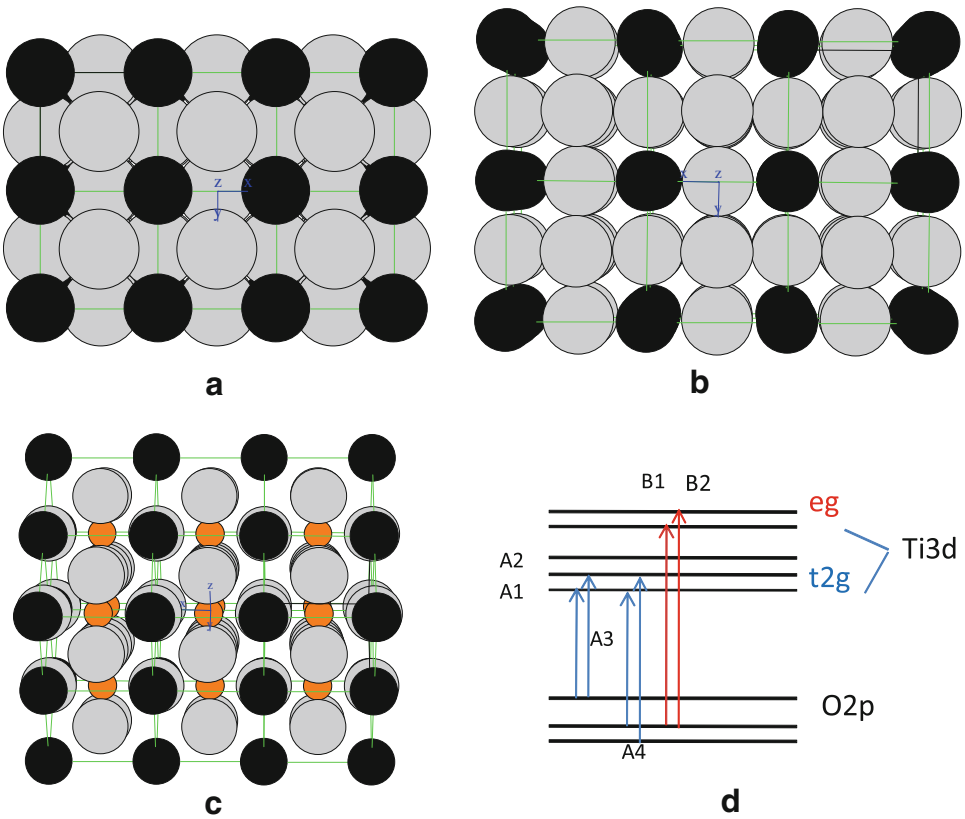

Fig. 1 Top view (**a**), side view (**b**) and perspective view (**c**) of $SrTiO_3$. Small black spheres (Sr^{2+}), large gray spheres (O^{2-}), smaller yellow spheres in **c** are those of Ti^{4+} cations. Also indicated in **d** are the electronic transitions between O2p and Ti3d levels (redrawn from Ref. [4])

production from water. It was found that bulk material (particles dimension >100 nm) was more active than 30 nm size particles which in turn were more active than 6.5 nm size particles (producing 28, 19.4 and 3 μmol of H_2 $g_{catal.}^{-1}$ h^{-1}, respectively [at 26.3 mW cm^{-2} with λ in the (250–380 nm)]. Reasons for this decrease are attributed to an increase in the water oxidation overpotential for the smaller particles and reduced light absorption due to quantum size effect. In another work [7], probing the anisotropy of the reactivity of $SrTiO_3$ microcrystals indicated that both reduced and oxidized products are formed preferentially on {100} surfaces. This anisotropy was explained as being due to differences in the electronic band structure. Because direct optical transitions for charge carriers having momentum vectors in the <100> direction overlap well with the spectral distribution of the absorbed photons, more photogenerated carriers are moving toward {100} surfaces than other surfaces and, as a result, the {100} surfaces are more active. Other work [8] has addressed the photocatalytic water splitting activity for hydrogen production over the mesoporous-assembled $SrTiO_3$ nanocrystal-based photocatalysts with various hole scavengers: methanol, ethanol, 2-propanol, D-glucose, and Na_2SO_3. Pristine mesoporous-assembled $SrTiO_3$ photocatalysts exhibited higher photocatalytic activity in hydrogen production than the non-mesoporous-assembled commercial photocatalysts or commercial $SrTiO_3$. These results indicate that the mesoporous assembly of nanocrystals with high pore uniformity plays a significant role, affecting the photocatalytic hydrogen production activity.

Moreover, it was seen that the Pt co-catalyst enhances the visible light harvesting ability of the mesoporous assembly with an optimum Pt loading of 0.5 wt% on the mesoporous-assembled $SrTiO_3$ photocatalyst providing the highest photocatalytic activity, with hydrogen production rate of 276 μmol h^{-1} $g_{catal.}$ and a quantum efficiency of 1.9 % under UV light irradiation. Other works indicated that Rh (1 %)-doped $SrTiO_3$ photocatalyst loaded with a Pt co-catalyst (0.1 wt%) gave 5.2 % of the quantum yield at 420 nm for the H_2 evolution reaction from a methanol solution (10 vol%) [9]. Another work [10] focused on doping $SrTiO_3/TiO_2$ with N ions (using hexamethylenetetramine) and optimized photocatalytic activity of hydrogen production (average hydrogen production rate = 5.1 mmol $g_{catal.}^{-1}$ h^{-1} with 2 wt% loaded Pt) under visible light was seen although little is known about the catalyst stability and comparison with the non-doped semiconductor material. A recent computational study (using the hybrid DFT method) of doping $SrTiO_3$ with metal cations coupled with experimental study showed that co-doping Cr and La ions had considerable enhancement effect on hydrogen production of water/methanol solution [11]. The reason invoked is that doping with La ions raised the Fermi level of Cr ions and stabilizes its oxidation state

of Cr^{3+} which is needed for the red shift of the band gap to extend light absorption into the visible region.

In this work, we have conducted a study of $Rh/SrTiO_3$ and $Pt/SrTiO_3$ materials in addition to monitoring their photo-catalytic reaction to further understand the extent of their activity. In particular, we attempt to answer which of the two metals is more active when added to the semiconductor support. We find that Rh has a weaker effect than Pt on hydrogen production (which is similar to the case where these metals are deposited on TiO_2 anatase [12]). Although we have not conducted detailed study of the particle size effect of the semiconductor, we do not find considerable difference in the reaction rates upon changing its morphology.

Experimental

$SrTiO_3$ was prepared by the sol–gel method where $TiCl_4$ was added to a strontium-nitrate solution in stoichiometric amounts. After the addition of $TiCl_4$ to the strontium-nitrate solution, the pH was raised with sodium hydroxide to a value between 8 and 9 where strontium hydroxide and titanium hydroxide precipitated. The precipitate was left to stand for about 12 h at room temperature to ensure completion of the reaction after which it was filtered and washed with de-ionized water until neutral pH ($\sim$7). The resulting material was then dried in an oven at 100 °C for a period of at least 12 h. Next the material was calcined at 800 °C. X-ray diffraction techniques were used to indicate formation of $SrTiO_3$ (Fig. S1). Several $SrTiO_3$ materials were tested in addition to a commercial $SrTiO_3$ (Sigma-Aldrich). Rh metals were impregnated from a solution containing $RhCl_3$ in 1 N HCl. The resulting catalyst differed from the initial $SrTiO_3$ as its particle size was far smaller and its BET surface area higher. Pt metals were impregnated the same manner (from a $PtCl_4$ precursor). Other techniques used to study the material included XPS, XRD, TEM, and UV–vis. Photoreaction was conducted in a batch reactor (100–250 mL) containing 10–25 mg of materials under stirring conditions with a UV lamp flux of about 1 mW cm^{-2}. Analysis was conducted using GC-TCD equipped with a Porapack Q with a N_2 carrier gas isothermally at 50 °C (N_2 flow rate = 20 mL min^{-1}). At these conditions, the products were eluted from the column with the following order: hydrogen, oxygen, methane, carbon dioxide, ethylene, ethane, propylene, propane, acetaldehyde, followed by ethanol. The powder XRD patterns of the samples were recorded on a Philips X'pert-MPD X-ray powder diffractometer. A 2θ interval between 10° and 90° was used with a step size of 0.010° and a step time of 0.5 s. The diffractometer was equipped with a Ni-filtered Cu K_α radiation source (λ = 1.5418 Å). The X-ray source was operated at 45 mA and 40 kV. Sample preparation for the X-ray analysis involved gentle grinding of the solid into a fine powder and packing of approximately 0.1–0.3 g of the sample into an aluminum sample holder with light compression to make it flat and tight. XRD patterns of the samples were recorded with the X'pert HighScore Plus software and saved in XRDML text format for further manipulation and processing. X-Ray Photoelectron spectroscopy was conducted using a Thermo Scientific ESCALAB 250 Xi, equipped with a monochromated AlK_α X-ray source, Ultra Violet He lamp for UPS, ion scattering spectroscopy (ISS), and reflected electron energy loss spectroscopy (REELS). The base pressure of the chamber was typically in the low 10^{-10} to high 10^{-11} mbar range. Charge neutralization was used for all samples (compensating shifts of $\sim$1 eV). Spectra were calibrated with respect to C1s at 284.7 eV. The Rh3d, Pt4f, O1s, Sr3d, Ti2p, C1s and valence band binding energy regions were scanned for all materials. Typical acquisition conditions were as follows: pass energy = 20 eV and scan rate = 0.1 eV per 200 ms. Ar ion bombardment was performed with an EX06 ion gun at 2 kV beam energy and 10 mA emission current; sample current was typically 0.9–1.0 μA. The sputtered area of 900 × 900 μm^2 was larger than the analyzed area: 600 × 600 μm^2. Self-supported oxide disks of approximately 0.5 cm diameter were loaded into the chamber for analysis. Data acquisition and treatment were done using the Avantage software.

Results

Figure 2 presents a TEM image of the $Rh/SrTiO_3$ catalyst. Rh particles with mean size of 3–4 nm are seen. $SrTiO_3$ is composed of small crystallites with sizes between 10 and 20 nm. The BET surface area of the material is found to be ca. 13 m^2 $g_{catal.}^{-1}$. Figure S2 presents high resolution image of an Rh particle; the spots in the FT image unambiguously identify it by its crystalline structure. Figure 3 presents TEM of two types of $Pt/SrTiO_3$: one where Pt was deposited on commercial $SrTiO_3$ and the other on $SrTiO_3$ that was prepared by the sol–gel method followed by annealing at 800 °C. The commercial $SrTiO_3$ is composed of particles with dimension larger than 1 μm while the one prepared by the sol–gel method is made of typical perovskite (cubic) particles with a mean size of about 50 nm; Pt particles cannot be seen at this resolution.

XP spectra Ti2p, Sr3d, O1s, and Rh3d (or Pt4f) were collected among other lines; here we focus on the main lines relevant to this study. Figure 4 presents XPS Rh3d and Ti2p of the as-prepared catalyst (a, b) and Ar ions sputtered (c, d). The presence of Rh^{3+} (mainly as Rh_2O_3) and Rh metal can be seen with binding energy = 307.0 and

308.8 eV, respectively, in line with reference elements [13]. To further confirm the presence of Rh metal as well to probe the extent of its reduction, the same area was Ar ions sputtered for 2 min (2 kV, 10 mA; sample current 10 mA). Clearly, the signal from Rh metal increased compared to that of Rh^{3+} due to reduction of Rh ions under bombardment. However, only about 50 % of Rh ions are reduced to metallic Rh. Our objective was not to reduce all Rh ions but to observe for the effects of mild ion sputtering on the reduction of the noble metal. Associated with Rh ions reduction is a reduction of Ti^{4+} ions to Ti^{3+} and Ti^{2+} ions (b, d) as has been seen in numerous work for Ar ions reduction of TiO_2 [14, 15].

Figure 5 presents the Sr3d, Ti2p and Pt4f of the as-prepared 0.5 wt% $Pt/SrTiO_3$ catalyst. Sr3d is typical of the doublet ($3d_{5/2}$, $3d_{3/2}$) of Sr^{2+} ions (spin orbit splitting close to 2 eV), the narrow lines of the $Ti2p_{3/2,1/2}$ and their binding energy positions indicate the absence of Ti^{3+} while the $Pt4f_{7/2,5/2}$ is that of metallic Pt (binding energy of $Pt_{7/2}$ at 72.5 eV with a spin orbit splitting of 3.4 eV). The presence of Pt metal in the as-prepared catalyst is in sharp contrast to that of the $Rh/SrTiO_3$ where a large fraction of Rh is found to be in the form or Rh^{3+} ions. This is typical of Pt deposited on reducible metal oxides where it is often largely present in its metallic form [16, 17].

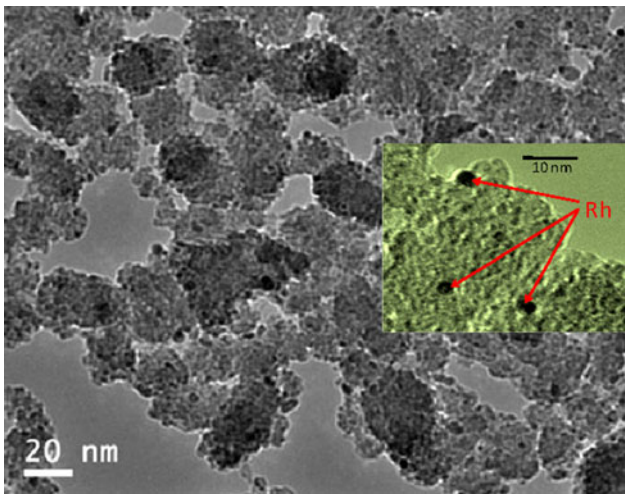

Fig. 2 TEM of 0.5 wt% $Rh/SrTiO_3$. Rh can be seen as dark particles in the main figure as well as the inset

Figure 6 presents results of the hydrogen production using photons of 3.3 eV in a batch reactor containing 0.5 wt% $Pt/SrTiO_3$ and 0.5 wt% $Rh/SrTiO_3$. Hydrogen production is seen together with methane. The production rate is comparable to that observed on Au/TiO_2 anatase previously and far higher than that of Au/TiO_2 rutile [18]. The ratio Rh/Ti is found equal to 0.07 while that of Pt/Ti is equal to 0.16. Two main observations are clear from Fig. 6. First $Pt/SrTiO_3$ is about six times higher than $Rh/SrTiO_3$ based on weight and about 20 times higher based on area. Even if we account for difference in the M to Ti^{4+} ratios, the rate of hydrogen production is still far higher for the Pt-containing catalysts compared to that of the Rh one. Second, $Rh/SrTiO_3$ produces large amounts of methane when compared to $Pt/SrTiO_3$. The larger amounts of methane can be rationalized by the fact that Rh is more active in breaking the C–C bond compared to Pt [19–21]. In this case, the ratio H_2 to CH_4 is equal to 2 for $Rh/SrTiO_3$ while it is equal to 8 in the case of $Pt/SrTiO_3$.

The reaction occurs due to electron excitation from the valence band (VB) O2p to the conduction band (CB) Ti3d upon UV illumination, as presented in Fig. 1. Alcohols are known as hole scavenges [22–24]. Ethanol is oxidized to acetaldehyde via two electron injection into the VB [25] with a time scale in the nanosecond range [26]. Mechanistically ethanol is first dissociatively adsorbed on the surface forming ethoxides (according to Eq. 2) and then upon two electron injections (through α-oxy radical [18, 25]) acetaldehyde is formed. The hydrogen ions released through this process are reduced to one hydrogen molecule [27, 28]. Reactions 1–4 represent these steps.

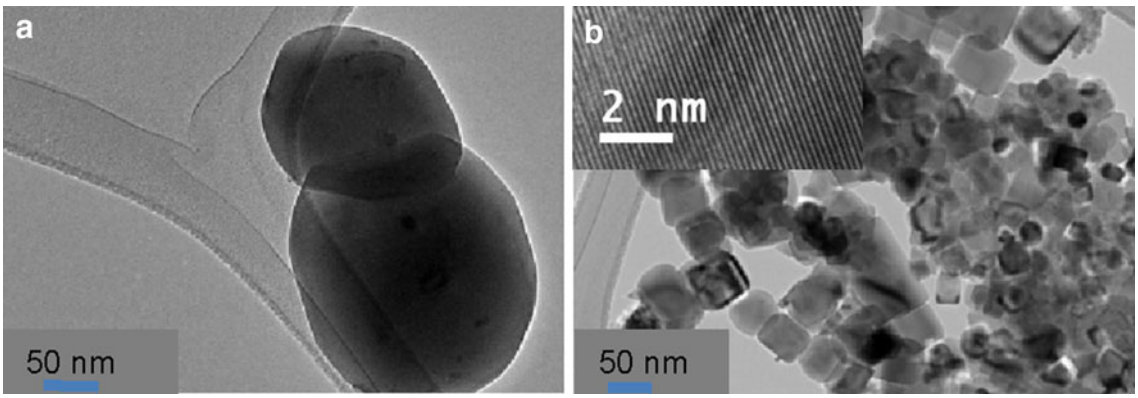

Fig. 3 TEM of 0.5 wt% $Pt/SrTiO_3$. **a** Commercial $SrTiO_3$ and **b** $SrTiO_3$ prepared by the sol–gel method; the *inset* in **b** presents the [100] cubic structure of $SrTiO_3$ evidence of a high degree of crystallinity

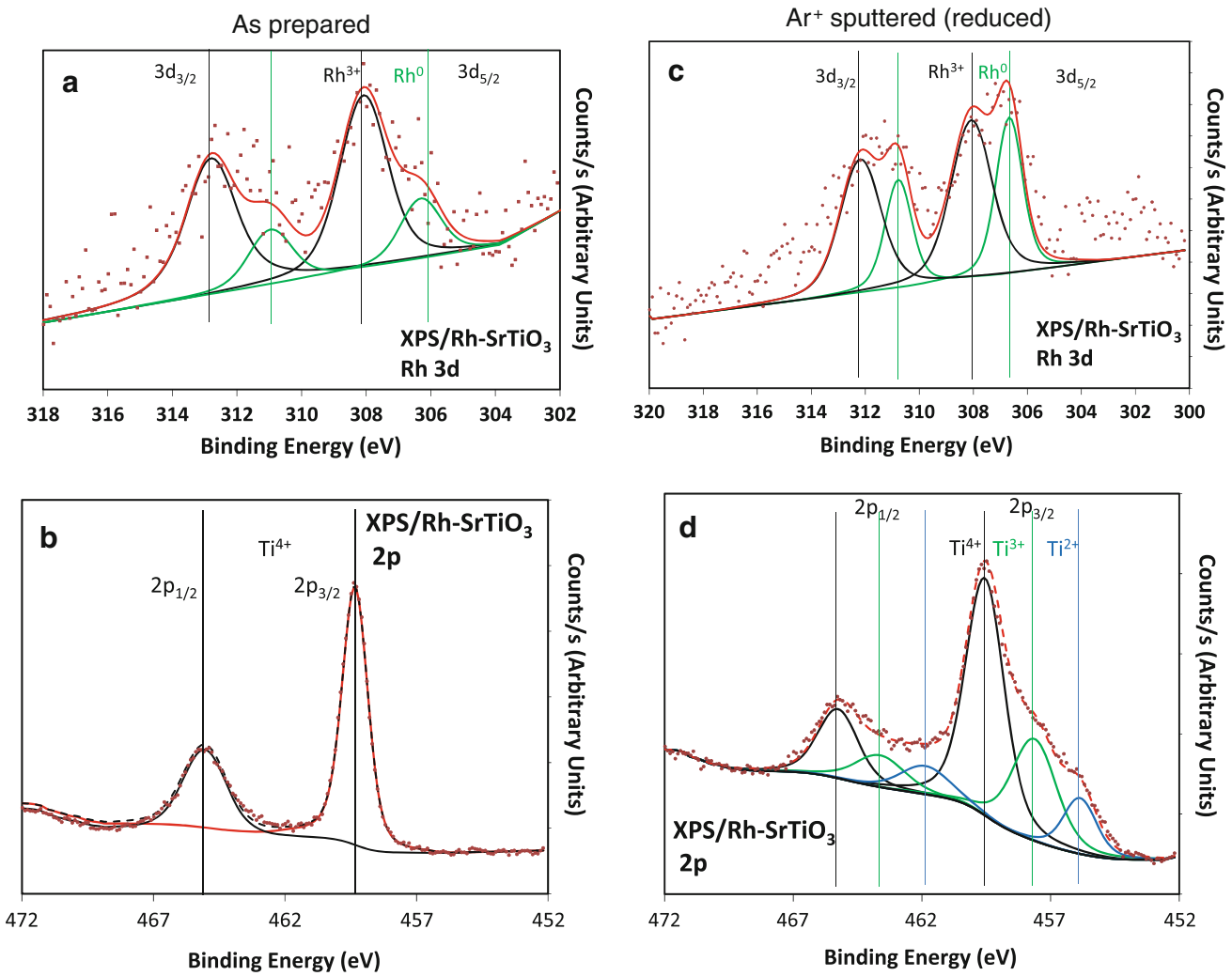

Fig. 4 XPS Rh 3d and Ti2p of 0.5wt% Rh/$SrTiO_3$. **a**, **b** As-prepared and **c**, **d** after Ar ions sputtering

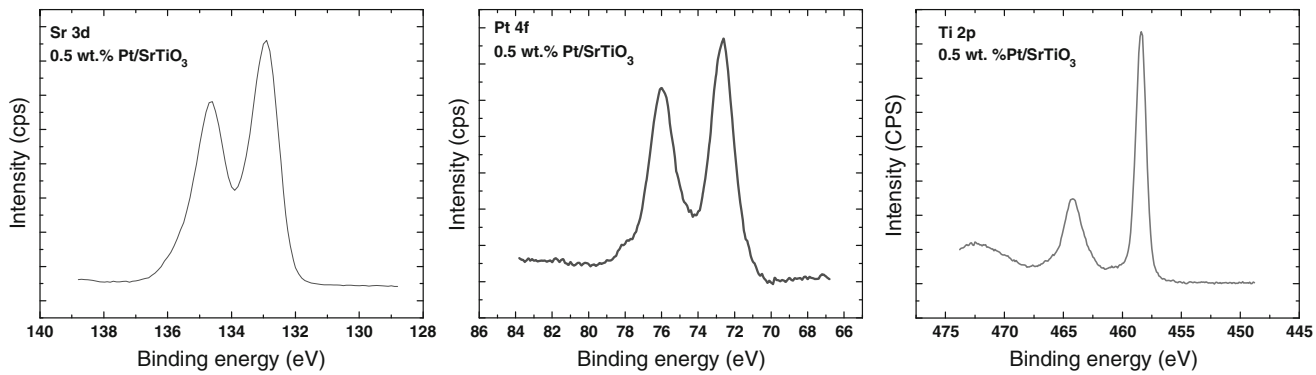

Fig. 5 XPS Sr3d, Ti2p and Pt 4f of the as-prepared 0.5 wt% Pt/$SrTiO_3$. The Sr to Ti atomic ratio is about 1

$$SrTiO_3 + UV \rightarrow e^- + h^+ \quad (1)$$

$$CH_3CH_2OH \rightarrow CH_3CH_2O(a) + H(a) \quad (2)$$

$$CH_3CH_2O(a) + 2h^+ \rightarrow CH_3CHO + H(a) \quad (3)$$

$$2H(a) + 2e^- \rightarrow H_2 \quad (4)$$

(a) adsorbed

The reaction over Pt/$SrTiO_3$ is similar to that over Au/TiO_2 where the main products are H_2 and acetaldehyde [1, 18], with traces of methane. However, over Rh/$SrTiO_3$ the reaction proceeds to CH_4. Therefore, a large fraction of CH_3CHO farther reacts with CH_4 and CO.

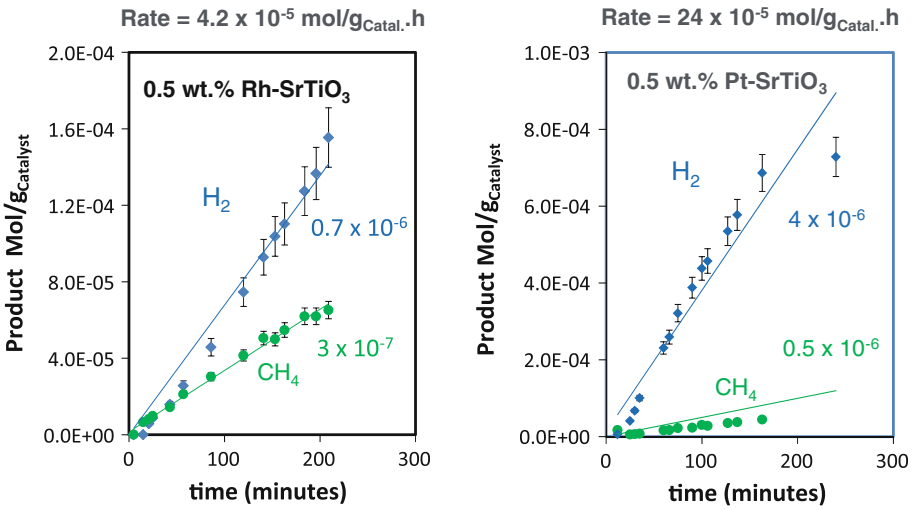

Fig. 6 Hydrogen and methane photo-production from ethanol over 0.5 wt% $Rh/SrTiO_3$ and 0.5 wt% $Pt/SrTiO_3$. BET surface area of $Rh/SrTiO_3 = 13\ m^2\ g^{-1}$ while that of $Pt/SrTiO_3$ is $3.5\ m^2\ g^{-1}$. The *numbers* inside the figure indicate the slope (the rate in moles of hydrogen per $g_{catal.}$ per minute)

$$CH_3CHO \rightarrow CH_4 + CO \quad (5)$$

As presented in Fig. 6, CH_4 is formed. Therefore, one should except if the reaction of Eq. 5 is complete, equal amounts of H_2 and CH_4 would be formed. We have conducted numerous runs and have found that in all cases CH_4 concentration was lower than that of H_2. Recent DFT studies on $SrTiO_3$ indicated the possibility of a pathway for ethanol decomposition involving CH_3CO radical (with the release of three hydrogen ions) [29]. In this case, CH_3CO may react with surface oxygen making acetate species or may split to CH_3 radical and CO; CH_3 radicals may react with OH radicals giving methanol, the latter would easily decompose to CO and hydrogen [30]. This route may explain the higher ratio H_2 to CH_4 observed. To extract all hydrogen atoms from ethanol, the formation of CH_4 is not desired and at present work is in progress to find a method to more efficiently break the carbon–carbon bond before obtaining acetaldehyde at 300 K under photon irradiation in the presence of water providing additional hydrogen and oxygen ions to complete the reforming reaction, as in high temperature ethanol steam reforming [31].

Conclusions

The rate of photo-catalytic reaction of ethanol to hydrogen is found to be far higher on $Pt/SrTiO_3$ compared to $Rh/SrTiO_3$. The most likely reason for the higher activity of the Pt containing catalysts is the ease by which metallic Pt is formed compared to Rh (where a large fraction of the as-prepared material is in Rh^{3+}). Ar ions sputtering $Rh/SrTiO_3$ considerably reduced Ti in $SrTiO_3$, but only reduced about half of Rh ions to metallic Rh. Another important difference is noticed between the two catalytic systems and it is related to reaction selectivity. $Rh/SrTiO_3$ produces large amounts of CH_4 compared to $Pt/SrTiO_3$; this is most likely related to the capacity of Rh to break the carbon–carbon bond compared to that of Pt.

References

1. Connelly KA, Idriss H (2012) The photoreaction of TiO_2 and Au/TiO_2 single crystal and powder surfaces with organic adsorbates. Emphasis on hydrogen production from renewables. Green Chem 14:260–280
2. Scott M, Idriss H (2009) Heterogeneous catalysis for hydrogen production. In: Anstis P, Crabtree RH (eds) Handbook of green chemistry—green catalysis, vol 1, chap. 10, ISBN-10: 3-527-31577-2
3. Yamada Y, Kanemitsu Y (2010) Band-to-band photoluminescence in $SrTiO_3$. Phys Rev B 82:121103 (R) 1–4
4. van Benthem K, Elsässer C, French R (2001) Bulk electronic structure of $SrTiO_3$: experiment and theory. J Appl Phys 90:6156–6164
5. Kudo A, Miseki Y (2009) Heterogeneous photocatalyst materials for water splitting. Chem Soc Rev 38:25–278
6. Townsend TK, Browning ND, Osterloh FE (2012) Nanoscale strontium titanate photocatalysts for overall water splitting. ACS Nano 6:7420–7426
7. Giocondia JL, Salvador PA, Rohrer GS (2007) The origin of photochemical anisotropy in $SrTiO_3$. Topics Catal. 44:529–533
8. Puangpetch T, Sreethawong T, Yoshikawa S, Chavadej S (2009) Hydrogen production from photocatalytic water splitting over mesoporous-assembled $SrTiO_3$ nanocrystal-based photocatalysts. J Mol Catal A Chem 312:97–106
9. Konta R, Ishii T, Kato H, Kudo A (2004) Photocatalytic activities of noble metal ion doped $SrTiO_3$ under visible light irradiation. J Phys Chem B 108:8992–8995
10. Jian-Hui Y, Yi-Rong Z, You-Gen T, Shu-Qin Z (2009) Nitrogen-doped $SrTiO_3/TiO_2$ composite photocatalysts for hydrogen production under visible light irradiation. J Alloy Compd 472:429–433

11. Reunchan P, Ouyang S, Umezawa N, Xu H, Zhang Y, Ye J (2013) Theoretical design of highly active $SrTiO_3$-based photocatalysts by a codoping scheme towards solar energy utilization for hydrogen production. J. Mater Chem A 1:4221–4227
12. Yang YZ, Chang CH, Idriss H (2006) Photo-catalytic production of hydrogen from ethanol over M/TiO_2 catalysts (M = Pd, Pt or Rh). Appl Cat B Environ 67:217–222
13. Briggs D, Seah MP (eds) Practical surface analysis, 2nd edn, vol 1. Wiley, Chichester
14. Idriss H, Barteau MA (1994) Characterization of TiO_2 surfaces active for novel organic syntheses. Catal Lett 26:123–139
15. Idriss H, Barteau MA (1994) Carbon-carbon bond formation on metal oxides: from single crystals toward catalysis. Langmuir 10:3693–3700
16. Yee A, Morrison S, Idriss H (2000) A Study of ethanol reactions over Pt/CeO_2 by temperature-programmed desorption and in situ FT-IR spectroscopy: evidence of benzene formation. J Catal 191:30–45
17. Chen H-W, Ku Y, Kuo Y-L (2007) Effect of Pt/TiO_2 characteristics on temporal behavior of o-cresol decomposition by visible light-induced photocatalysis. Water Res 41:2069–2078
18. Murdoch M, Waterhouse GIN, Nadeem MA, Metson JB, Keane MA, Howe RF, Llorca J, Idriss H (2011) The effect of gold loading and particle size on photocatalytic hydrogen production from ethanol over Au/TiO_2 nanoparticles. Nat Chem 3:489–492
19. Idriss H (2004) Ethanol reactions over the surfaces of noble metal/cerium oxide catalysts. Platinum Metals Rev. 48:105–115
20. Idriss H, Scott M, Llorca J, Chan S.C, Chiu W, Sheng PY, Yee A, Blackford MA, Pas SJ, Hill AJ, Alamgir FM, Rettew R, Petersburg C, Senanayake SD, Barteau MA (2008) A phenomenological study of the metal–oxide interface: the role of catalysis in hydrogen production from renewable resources. Chem Sus Chem 1:905–910
21. Chen H-L, Liu S-H, Ho J-J (2006) Theoretical calculation of the dehydrogenation of ethanol on a Rh/CeO_2 (111) surface. J Phys Chem B 110:14816–14823
22. Muir JMR, Choi YM, Idriss H (2012) DFT study of ethanol on TiO_2 (110) rutile surface. Phys Chem Chem Phys 14: 11910–11919
23. Yu Z, Chuang SSC (2007) In situ IR study of adsorbed species and photogenerated electrons during photocatalytic oxidation of ethanol on TiO_2. J Catal 246:118–126
24. Wu G, Chen T, Zong X, Yan H, Ma G, Wang X, Xu Q, Wang D, Lei Z, Li C (2008) Suppressing CO formation by anion adsorption and Pt deposition on TiO_2 in H_2 production from photocatalytic reforming of methanol. J Catal 253:225–227
25. Mller BR, Majoni S, Memming R, Meissner D (1997) Particle size and surface chemistry in photoelectrochemical reactions at semiconductor particles. J. Phys. Chem. B 101:2501–2507
26. Hoffmann MR, Martin ST, Choi W, Bahneman DW (1995) Environmental applications of semiconductor photocatalysis. Chem Rev 95:69–96
27. Nadeem MA, Murdoch M, Waterhouse GIN, Metson JB, Keane MA, Llorca J, Idriss H (2010) Photoreaction of ethanol on Au/TiO_2 anatase. Comparing the micro to nano particle size activities of the support for hydrogen production. J Photochem Photobiol A Chem 216:250–255
28. Bowker M, Davies PR, Al-Mazroai LS (2009) Photocatalytic reforming of glycerol over gold and palladium as an alternative fuel source. Catal Lett 128:253–255
29. Adeagbo WA, Fischer G, Hergert W (2011) First-principles investigations of electronic and magnetic properties of SrTiO3 (001) surfaces with adsorbed ethanol and acetone molecules. Phys Rev B 83:195428-1–195428-8
30. Bowker M, James D, Stone P, Bennett R, Perkins N, Millard L, Greaves J, Dickinson A (2003) Catalysis at the metal-support interface: exemplified by the photocatalytic reforming of methanol on Pd/TiO_2. J Catal 217:427–433
31. Scott M, Geoffrey M, Chiu W, Blackford MA, Idriss H (2008) Hydrogen production from ethanol over Rh-Pd/CeO_2 catalysts. Topics Catal. 51:39–48